

Observational evidence for the link between the variable optical continuum and the jet of a radio-loud galaxy 3C 390.3

Tigran G. Arshakian¹, Andrei P. Lobanov¹, Vahram H. Chavushyan^{2,3}, Alla I. Shapovalova⁴, and J. Anton Zensus¹

¹ Max-Planck-Institut für Radioastronomie, Auf dem Hügel 69, 53121 Bonn, Germany
e-mail: tigar@mpi-fr-bonn.mpg.de

² Instituto Nacional de Astrofísica Óptica y Electrónica, Apartado Postal 51 y 216, 72000 Puebla, Pue, México

³ Instituto de Astronomía, UNAM, Apartado Postal 70-264, 04510 México D.F., México

⁴ Special Astrophysical Observatory of the Russian AS, Nizhnij Arkhyz, Karachaevo-Cherkesia 369167, Russia

Received ;date; / Accepted ;date;

ABSTRACT

Context. The “central engine” of AGN is thought to be powered by accretion on a central nucleus believed to be a super-massive black hole. The localization and exact mechanism of the energy release in AGN are still not well understood.

Aims. We present observational evidence for the link between variability of the radio emission of the compact jet, optical and X-ray continua emission and ejections of new jet components in the radio galaxy 3C 390.3.

Methods. The time delays between the light curves of the individual jet components and the light curve of the optical continuum are estimated by using minimization methods and the discret correlation function.

Results. We find that the variations of the optical continuum are correlated with radio emission from a stationary feature in the jet. This correlation indicates that the source of variable non-thermal continuum radiation is located in the innermost part of the relativistic jet.

Conclusions. We suggest that the continuum emission from the jet and counterjet ionizes material in a subrelativistic outflow surrounding the jet, which results in a formation of two conical regions with broad emission lines (in addition to the conventional broad line region around the central nucleus) at a distance ≥ 0.4 parsecs from the central engine. Implications for modeling of the broad-line regions are discussed.

Key words. galaxies: active – galaxies: jets – galaxies: nuclei – galaxies: individual: 3C 390.3 – radiation mechanisms: non-thermal

1. Introduction

The variable continuum flux in AGN, signaling the activity of the central engine, is detected throughout the entire electromagnetic spectrum, on time-scales from days to years (Peterson et al. 2002; Zheng 1996; Wamsteker et al. 1997; Shapovalova et al. 2001). The continuum flux is believed to be responsible for ionizing the cloud material in the broad-line region (BLR). Localization of the source of the variable continuum emission in AGN is therefore instrumental for understanding the mechanism for release and transport of energy in active galaxies. In radio-quiet AGN, representing about 90 % of the AGN population, the presence of rapid X-ray flux variations and iron emission line (Fe K α) indicates that most of the soft X-ray emission originates from the accretion disk (Mushotzky et al. 1993). In radio-loud AGN, the activity of the central engine is accompanied by highly-relativistic collimated outflows (jets) of plasma material formed and accelerated in the vicinity of the black hole (Ferrari 1998). Inhomogeneities in the jet plasma appear as a series of compact radio knots

(jet components) observed on scales ranging from several light weeks to about a kiloparsec (Alef et al. 1996; Kellermann et al. 2004). Continuum emission from the relativistic jet dominates at all energies (see Ulrich et al. 1997; Worrall 2005), swamping the X-ray emission associated with the accretion flow. Hence, the continuum variability in radio-loud AGN may be related to both the jet and the instabilities of accretion flows (Mushotzky et al. 1993; Ulrich et al. 1997) near the central engine. The unification scheme (Urry & Padovani 1995) of radio-loud AGN suggests that the central powerful optical continuum and broad emission lines are viewed directly in radio quasars and BL Lacs, whereas in radio galaxies these can be hidden by an obscuring, dusty torus, and therefore, the bulk of continuum and broad-line emission in radio galaxies may be attributed to the relativistic jet rather than the central engine. The presence of a positive correlation between beamed synchrotron emission from the base of the jet and optical nuclear emission in radio galaxies suggests that the optical emission is non-thermal and may originate from a relativistic jet (Chiaberge et al. 1999, 2002; Hardcastle & Worrall 2000). The detection of a correlation between the radio and optical emission variability from the nuclear region would be the most direct evidence of opti-

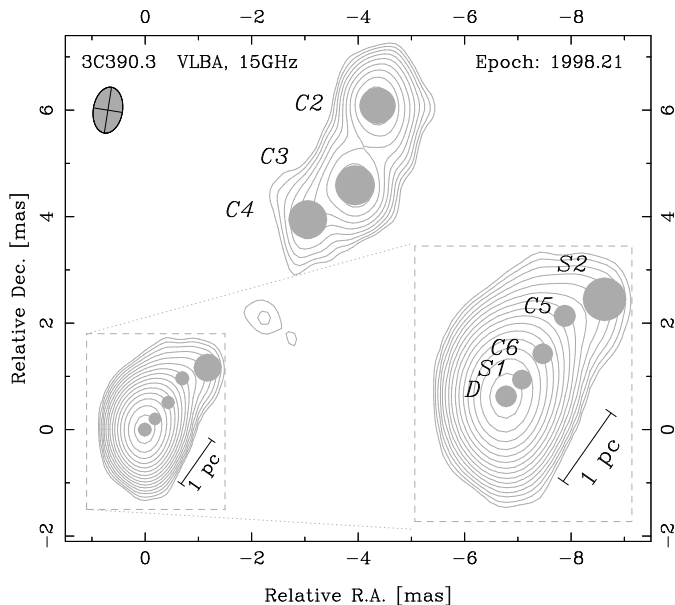


Fig. 1. Radio structure of 3C 390.3 observed in 1998.21 with very long baseline interferometry at 15 GHz (2 cm). Innermost fraction of the jet is shown in the inset. The resolving point-spread function (beam) plotted in the upper left corner is 0.87×0.55 mas oriented at an angle of 8.0 degrees (clockwise rotation). The peak flux density in the image is 190 mJy/beam (3.1×10^9 K) and the rms noise is 0.2 mJy/beam ($1 \text{ Jy} = 10^{-26} \text{ W m}^{-2} \text{ Hz}^{-1}$). The contours are drawn at 1, $\sqrt{2}$, 2... of the lowest contour shown at 0.6 mJy/beam. The structure observed is quantified by a set of two-dimensional, circular Gaussian features (shaded circles) obtained from fitting the visibility amplitudes and phases (Pearson 1997). Similar fits have been obtained for ten observations from the 15 GHz VLBA survey database (Kellermann et al. 2004), for the purpose of cross-identifying and tracing different features in the jet. The labels mark three stationary features (D, S1, and S2) and a subset of moving components (C2–C6) identified in the jet. Note that two more components, C7 and C8, have been first identified in the jet in the VLBA images at later epochs (see Fig. 2).

cal continuum emission coming from the jet. No observational evidence has yet been reported for a link between optical/UV continuum variability and the radio jet in radio-loud AGN. In Section 2, we analyse the structure and kinematics of the pc-scale jet in 3C 390.3 and look for correlations between variable emission of jet components and nuclear optical emission on scales less than one parsec. The structure and emission mechanism of the sub-parsec-scale region around the central nucleus is discussed in Section 3. In Section 4, we discuss the results and draw conclusions.

2. The link between radio jet and optical continuum in the radio galaxy 3C 390.3

To search for a relation between variability of the continuum flux and changes in the radio structure in AGN on scales of ~ 1 pc ($1 \text{ pc} = 3.086 \times 10^{16} \text{ m}$), we combine the results from monitoring of the radio-loud broad emission-

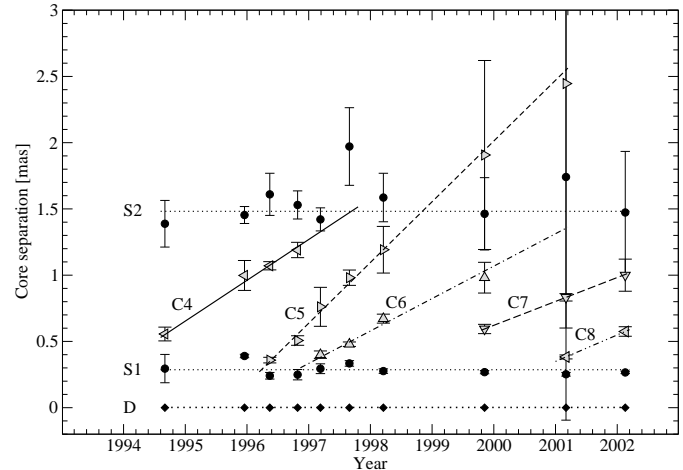


Fig. 2. Separation of the jet components relative to the stationary feature D (filled diamonds) for ten epochs of VLBI observations. Moving components are denoted by leftward triangles (C4), rightward triangles (C5), upward triangles (C6), downward triangles (C7), leftward triangles (C8), and stationary components S1 and S2 are marked by filled circles. The lines represent the best linear least-squares fits to the component separations.

line galaxy 3C 390.3 (redshift $z = 0.0561$) in the optical (Shapovalova et al. 2001; Sergeev et al. 2002), UV (Zheng 1996), and X-ray (Leighly et al. 1997) regimes with ten very long baseline interferometry (VLBI) observations of its radio emission at 15 GHz (Kellermann et al. 2004) made from 1992 to 2002 using the VLBA¹.

2.1. Structure and kinematics of the parsec-scale jet

To parameterize the structure of the radio emission, we applied the technique of modelfitting (Pearson 1997) and fit interferometric visibilities from each of the ten VLBA datasets by a set of circular Gaussian components (Fig. 1 and Table 1 in the Appendix) and used the positions and flux densities of these components for tracing the evolution of the jet emission on angular scales of ~ 3 milliarcseconds (mas). At the distance of 3C 390.3, 1 mas corresponds to a linear distance of 1.09 pc for the flat cosmology with the Hubble constant $H_0 = 70 \text{ km s}^{-1} \text{ Mpc}^{-1}$ and the matter density $\Omega_m = 0.3$.

From the component separations measured within 3 mas from the feature D at the narrow end of the jet (Fig. 1), we identified five moving components C4–C8 (in addition to the previously known components C2 and C3; Alef et al. 1996) and two stationary features S1 and S2 separated from D by 0.28 ± 0.03 mas and 1.50 ± 0.12 mas, respectively (Fig. 2). The more distant stationary feature S2 can be explained by a small change in the direction of the flow that causes the relativistic dimming of the radio emission (Gomez et al. 1997). The presence of S1 may be related to both geometrical and physical factors. Linear fits to the observed separations of the compo-

¹ Very Long Baseline Array of National Radio Astronomy Observatory, Socorro, NM, USA

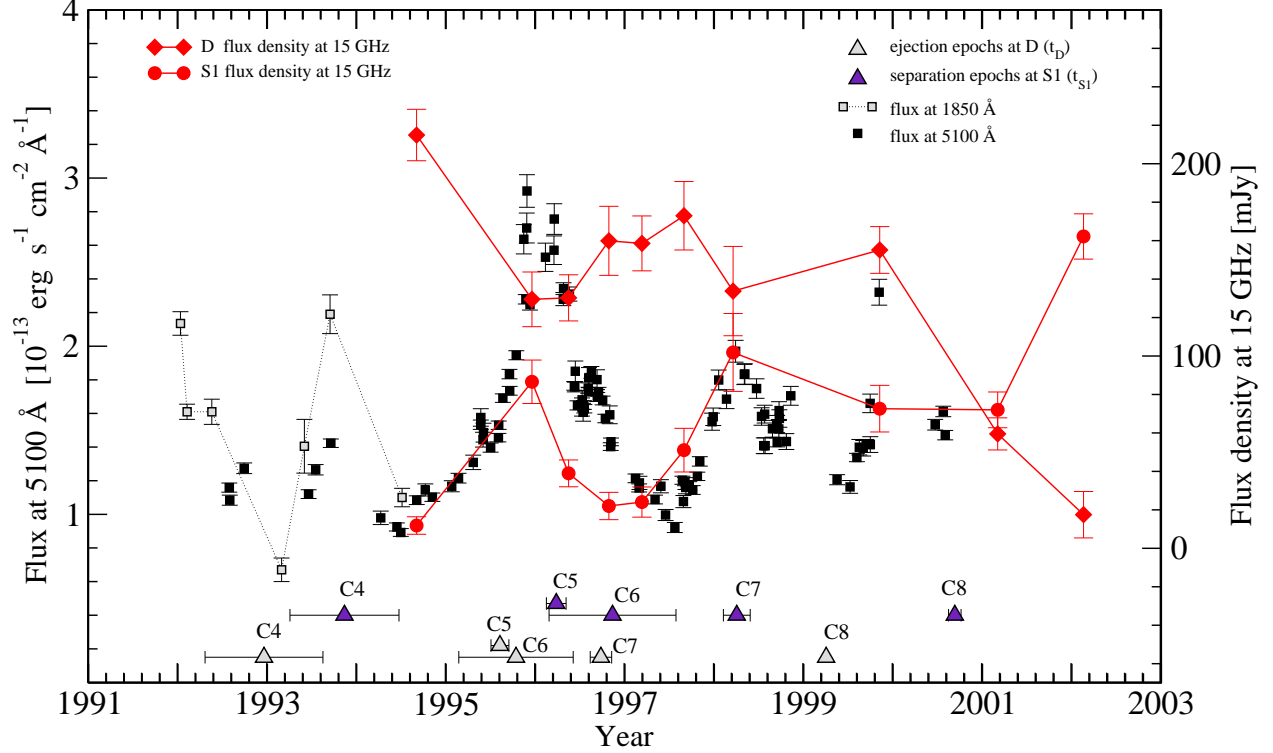


Fig. 3. The variations of the continuum fluxes of 3C 390.3 during the 1992 to 2002.2 time period. Optical continuum light curve at 5100Å (Shapovalova et al. 2001; Sergeev et al. 2002) (black squares), UV continuum fluxes (Zheng 1996) scaled by a factor of 50 (grey squares), and variations of radio flux density from D and S1 components (filled red diamonds and circles) are presented. The times of ejection, t_D , of radio knots from D (presumed base of the jet) and the times of their separation, t_{S1} , from the component S1 are marked by open triangles and filled triangles respectively.

nent C4–C8 from the component D yield proper motions of 0.2–0.4 mas/yr, which correspond to apparent speeds of 0.8–1.5 c , where c is the speed of light. Back-extrapolation of the fits to C5 and C6 indicates that these two components may originate from a single event. They could result from a moving perturbation in the jet that creates a forward and a reverse shock pair (Gomez et al. 1997). We used the linear fits to estimate, for each moving component, the epoch, t_D , at which it was ejected from the component D and the epoch, t_{S1} , when it passed through the location of the stationary feature S1 (see Figs. 2 and 3).

2.2. Correlations between variable emission of jet components and optical continuum

In Fig. 3, the properties of the components D and S1 identified in the radio jet of 3C 390.3 are compared with the optical continuum emission at 5100Å (Sergeev et al. 2002; Shapovalova et al. 2001) and 1850Å (Zheng 1996). The radio fluxes from D (f_D) and S1 (f_{S1}) features (Fig. 3) show an ap-

parent anticorrelation during 1996.4–2002.2 time period, which indicates that there should be a time delay between radio light curves. We should expect that the radio flare propagates downstream of the jet, and hence the D component should be the leading source of emission.

A poor radio sampling (10 points) makes it impossible to use the discrete correlation or cross-correlation functions for determining the time delay τ_{D-S1} between f_D and f_{S1} (hereafter in the subscripts of τ the first term indicates the leading source). Here, we employ the χ^2 minimization method for linearly interpolated radio light curves. Each light curve is linearly interpolated, and the data points of one light curve are shifted. For every value of the shift we calculate the normalized $\chi^2/(N-n)$, where N is the number of overlapping points and $n = 2$ is the number of fitted parameters. Application of this method shows that the best time delay is $\tau_{D-S1} \sim 1$ yr (Fig. 4) for both the entire radio data and for a subsample of eight radio observations made during the time period of optical measurements (from 1994.6 to 2000.6). The time delay of ~ 1 yr is comparable with the mean time $t_{D-S1} = 1.04 \pm 0.16$ yr at which the moving

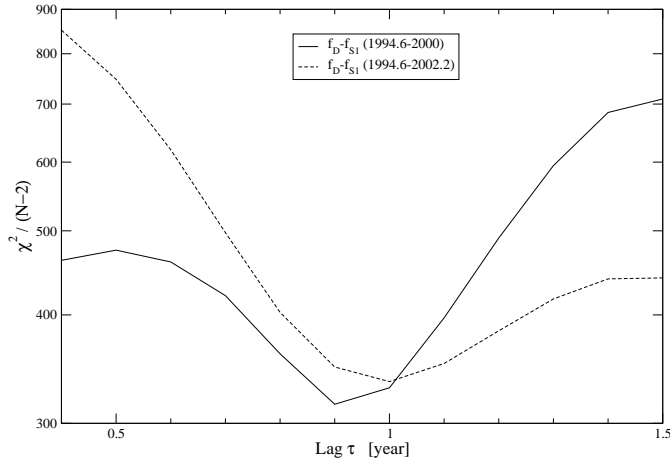


Fig. 4. The normalized χ^2 statistics as a function of time delay between radio light-curves (ten data points between 1994.6 and 2002.2) of D and S1 components. This dependence is presented for the entire radio data (dashed line) and for a subsample of eight radio epochs between 1994.6 and 2000 (solid line). The minimum corresponds to the best-fit delay. The best-fit delays are found in the range between 0.9 years to 1 year.

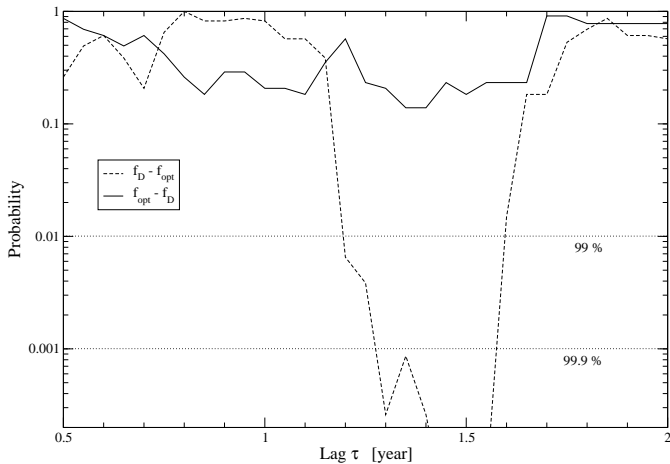


Fig. 5. The significance level of the Spearman's rank correlation coefficient for different time delays between f_D and f_{opt} (dashed line) and f_{opt} and f_D (solid line) light curves. The horizontal dotted lines correspond to the 99 % and 99.9 % confidence levels.

components C4-C7 (the data for C8 are too sparse for making reliable estimates) pass the distance between D and S1. This indicates that the time delay between variations of radio light curves is related to the passage of moving components between D and S1 stationary components.

We use a different method to check for correlations between variability of the jet radio emission and the optical continuum emission at 5100\AA (f_{opt}). Using the advantage of a dense sampling of optical measurements we generate paired radio-optical data points. For every value of time shift and for every radio measurement we assign an optical flux which is linearly interpolated between two nearest epochs of optical observations around the shifted epoch of a radio measurement. The signif-

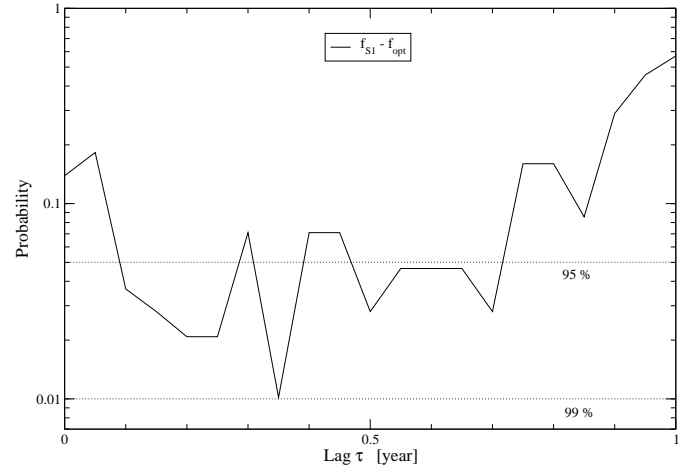


Fig. 6. The significance level of the Spearman's rank correlation coefficient for different time delays between f_{S1} and f_{opt} light curves. The horizontal dotted lines correspond to the 95 % and 99 % confidence levels.

icance level of the Spearman's rank correlation coefficient is calculated for different values of the shift.

This method has been applied to the optical (106 points) and radio (eight points) data measured between 1992 and 2002. Correlations have been searched between the optical continuum and radio emission from the components D, S1, S2, and from a composite flux from D+S1. No significant correlation exists for the moving features, the stationary feature S2 and the flux density of D+S1 (not shown in Fig. 3). A significant correlation ($> 99\%$, see Fig. 5) is present between f_D and f_{opt} for time lags ranging from $\tau_{D-opt} \sim (1.2 - 1.6)$ yr. No significant correlation is found in the $f_{opt} - f_D$ relation plane where the optical continuum is assumed to lead the radio emission (Fig. 5). This result strongly suggests that the radio emission precedes the optical continuum by approximately 1.4 yr, and that there should be a physical relation between variable radio emission from the feature D of the jet and optical continuum emission. One should expect that the optical continuum also correlates with and follows the radio emission of S1 component with time delay of $\tau_{S1-opt} = \tau_{D-opt} - \tau_{D-S1} \sim 0.4$ yr. Fig. 6 shows that there is a positive correlation (at the $\geq 95\%$ confidence level) in the $f_{S1} - f_{opt}$ relation plane for a wide range of time lags from ~ 0 yr to ~ 0.7 yr. To check this result we use the discrete correlation function (Edelson & Krolik 1998) which yields a strong positive correlation between the radio flux density of S1 (leading source) and the optical continuum for time lags ranging between 0 yr and 0.8 yr with slightly larger correlation function at small time delays, $\sim (0 - 0.4)$ yr (see Fig. 7). Both statistical tests show a positive correlation between variations of f_{S1} and f_{opt} for $\tau_{S1-opt} \sim (0 - 0.7)$ yr. It is most probable that the optical continuum is produced near or at the location of the radio emission (0-0.4 light year from the feature S1). If the optical continuum trails the radio emission then the optical and high-energy photons are likely to be produced by Compton up-scattering of radio photons by the relativistic electrons of the jet (Ulrich et al. 1997). In either case, the size of the region from which the optical continuum is emitted should be very small.

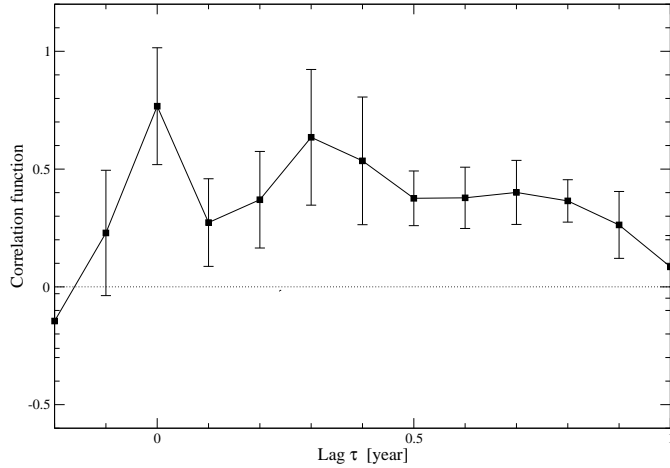


Fig. 7. The discrete correlation function for different lags between f_{S1} and f_{opt} during the 1994.5 to 2000 time period. The 0.1 year bin width of the time delay is adopted to minimize the errors of correlation function. 1σ error bars are presented.

This can also be deduced from the facts that, in 3C 390.3, the changes of the optical flux at 5100 \AA follow the variations in the UV and soft X-ray emission, with time delays of about 5 ± 5 days (Dietrich et al. 1998) and the overall spectrum in the optical to soft X-ray range is represented by a single power-law with a spectral index $\alpha = 0.89$ (Wamsteker et al. 1997). These observations indicate that a large fraction of the variable continuum emission is non-thermal and it is produced in a region of ~ 5 light days (0.004 pc) in size.

The link between the optical continuum and the component S1 in the radio jet is further supported by the correlation between the continuum light curve and the characteristic epochs t_D and t_{S1} of the moving components C4–C7. For the components C4–C7, the epochs t_{S1} of separation from the stationary feature S1 are coincident, within the errors, with the maxima in the optical continuum (Fig. 3). All four ejection events occur within $\sim 0.3 \text{ yr}$ after a local maximum is reached in the the intensity of the optical continuum (the average time delay between the maxima and the epochs t_{S1} is $0.18 \pm 0.06 \text{ years}$). The null hypothesis that this happens by chance is rejected at a confidence level of 99.98%. This suggests that radio ejection events of the jet components are coupled with the long-term variability of optical continuum.

3. The central sub-parsec-scale region

The link between the radio emission from D and S1 suggests that the appearance of these stationary features in the jet is due to physical, rather than geometrical, factors. The location of stationary features with respect to the central nucleus is important for understanding the structure of the central engine and its radiation mechanism producing the variable continuum emission. If the component D is identified with the proverbial “base” of the counterjet then the component S1 should be the base of the jet. We should expect that $f_D < f_{S1}$ because of relativistic Doppler effect. The fact that $f_D \gtrsim f_{S1}$ during the six year time period (Fig. 3) rules out the assumption that D is the base

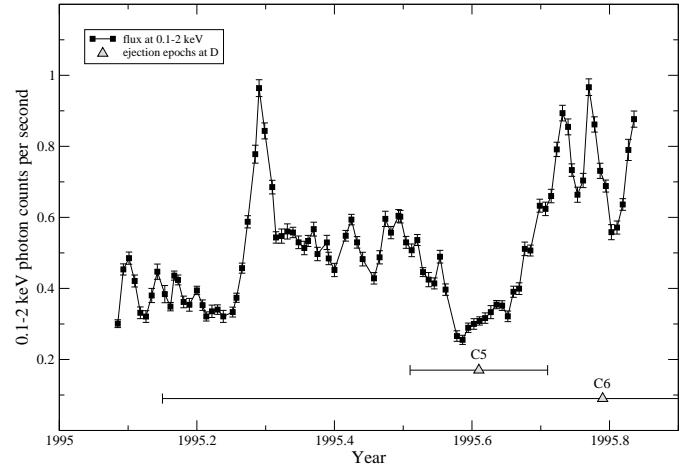


Fig. 8. The variations of soft X-ray fluxes at 0.1-2 keV Leighly et al. (1997) for 3C 390.3 between 1995 and 1996 superimposed with the epochs of origin of C5 and C6. 1σ error bars are presented for all data.

of the counterjet. The component D is likely to be the base of the VLBI jet near the central engine; the base being the location at which the flow either becomes supersonic (Daly et al. 1988) or optically thin (Königl 1981; Lobanov 1998) or releases the energy contained in the Poynting flux (Romanova & Lovelace 1996). The identification of the component D with the central engine is supported by the correlation between the ejection epoch, t_D , of the component C5 and the variability of the X-ray flux at 0.1-2 keV (Fig. 8). The ejection of C5 occurred after a dip in the X-ray emission and hardening of the spectrum (Leighly et al. 1997) suggesting (similar to 3C 120; Marscher et al. 2002) that the soft X-ray emitting disk material disappears into the black hole and a fraction of the infalling matter is ejected into the jet. The component D should then be associated with the radio emission coming from the immediate vicinity of the central engine of 3C 390.3 (assuming that absorption along the line of sight passing through outer layers of the torus is sufficiently weak). This emission is probably generated in or above a hot corona at a distance $\geq 200 R_s$ above the accretion disk (Fabian 2004; Ponti et al. 2004) ($R_s = 2GM_{bh}/c^2$ is the Schwarzschild radius for a black hole of mass M_{bh} , where G is the Newtonian gravitational constant).

The component S1 then can be associated with the stationary radio feature which may be produced by the internal oblique shock formed in the continuous relativistic flow (Gomez et al. 1995). In this scenario, the energy release in the form of variable radiation can be produced by interaction of relativistically moving compact component or shock (?) with the *stationary shocks* (Gomez et al. 1995) produced at the positions of D and S1 of the jet. The time delay between variations of f_D and f_{S1} is equal to the time ($\tau_{D-S1} = t_{D-S1}$) at which the ejected component passes from D to S1. This is in fact the case for the 3C 390.3 ($1 \text{ yr} \approx 1.04 \text{ yr}$, see the previous section). The characteristics of a long-term variability of optical continuum flux (amplitude of optical flares and their rate) are likely to be related to the properties of the jet such as the jet ejection rate, structure and kinematics of the sub-parsec scale jet.

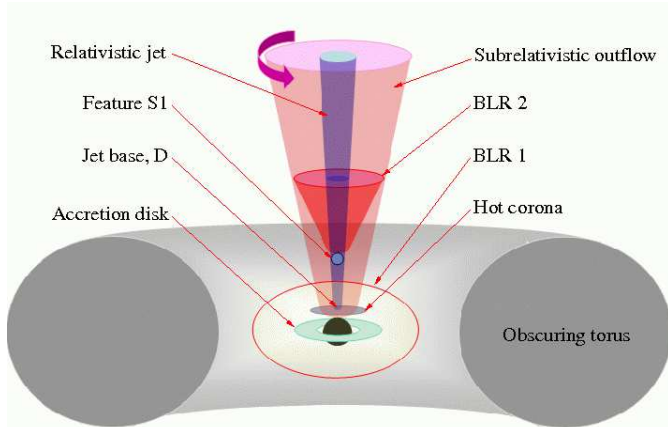


Fig. 9. A sketch of the nuclear region in 3C 390.3. The drawing is made not to scale and shows only the approaching jet. The broad-line emission is likely to be generated both near the disk (Peterson et al. 2002) (BLR 1, ionized by the emission from a hot corona (Fabian 2004; Ponti et al. 2004) or the accretion disk; Field & Rogers 1993) and in a rotating subrelativistic outflow (Murray et al. 1997; Proga et al. 2000) surrounding the jet (BLR 2, ionized by the emission from the relativistic plasma in the jet).

The results presented above imply strongly that the bulk of variable optical continuum and the broad-line emission associated with it are generated at a large distance from the central engine (in addition to the likely contributions from the hidden, “conventional” BLR close to the nucleus). Adopting an angle² of 50° between the jet and the line of the sight, the corresponding de-projected distance between D and S1 is $0.3 \text{ pc} / \sin 50^\circ \approx 0.4 \text{ pc}$. The optical continuum emission of 3C 390.3 leads the double-peaked $H\beta$ line emission by ~ 30 – 100 days (Shapovalova et al. 2001; Sergeev et al. 2002). The localization of the source of optical continuum with the innermost part of the jet near S1 implies that the broad line emission originates in the cone within ~ 100 light days at a distance $\geq 0.4 \text{ pc}$ from the central engine. The conical shape of the BLR associated with the outflow arises from a large fraction of the continuum radiation being beamed into a cone with a half-opening angle² $\psi \approx 30^\circ$.

The structure of the nuclear region implied by the results presented above is sketched in Fig. 9. In 3C 390.3, the changes in the blue and red wings of $H\beta$ emission line occur quasi-simultaneously (Shapovalova et al. 2001) implying that broad-line region associated with the component S1 (outflow related BLR 2 in Fig. 9) is shaping both the blue and red wings (otherwise one should expect significant time delay between the variability of the wings). The observed double-peaked structure of the $H\beta$ line can be reproduced by a rotation of the approaching jet and a subrelativistic outflow (Murray et al. 1997;

Proga et al. 2000). BLR 2 is evident in the broad-line emission at times when the jet emission dominates the optical continuum (see Fig. 3). BLR 1 may be manifested in the broad-line emission around the epochs of minima in the continuum flux, when the jet contribution to the ionizing continuum is small.

4. Discussion and conclusions

The large distance of the BLR 2 from the central engine challenges the existing models in which the broad-line emission is localized exclusively around the disk or near the central engine (Peterson et al. 2002). It also questions the assumption of virialized motion in the BLR (Kaspi et al. 2000), which forms the foundation of the method for estimating black hole masses from reverberation mapping (Peterson et al. 2002). Time delays and profile widths measured during periods when the jet emission is dominant may not necessarily reflect the Keplerian motion in the disk, but rather trace the rotation and outward motion in an outflow. This can result in large errors in estimates of black hole masses made from monitoring of the broad-line emission. In the case of 3C 390.3, the black hole mass (2.1×10^9 solar masses, M_\odot) estimated effectively from the measurements near the maximum in the continuum light curve (Shapovalova et al. 2001) is significantly larger than the values (3.5 – $4 \times 10^8 M_\odot$) reported in other works (Wandel et al. 1999; Kaspi et al. 2000). This difference is reconciled by considering the line width and the time delay between the optical continuum and line fluxes near the minimum of the continuum light curve, which yields $M_{\text{bh}} = 3.8 \times 10^8 M_\odot$. The possible existence of an outflow-like region in a number of radio-loud AGN should be taken into account when estimates of the nuclear mass are made from the variability of broad emission lines.

While the continuum emission at the base of the counterjet is likely to be too weak to be detected because of the relativistic dimming and large opacity in the disk, the optical/UV/X-ray line emissions from BLR 2 in the counterjet are free from relativistic effects and have better chances to penetrate the absorbing medium towards the observer. Detection of a time lag between correlated variability of emission lines from the far-side and near-side BLRs would be the most direct observational evidence for double BLRs ionized by the continuum radiation from the bases of the jet and counterjet. If the jets are intrinsically symmetric then a time delay of ~ 2 years is expected for such variations in 3C 390.3 (assuming the distance of $\sim 1 \text{ pc}$ between oppositely positioned BLRs and the jet viewing angle of 50°).

The presence of the BLR2 in radio-loud AGN is capable of explaining some of the spectral characteristics of emission lines. Depending on the orientation of the jet, the approaching and rotating outflow material in the BLR2 will imprint prominent signatures on the emission lines. At small viewing angles of the jet the BLR2 may produce blueshifted and single-peaked broad emission lines, while non-shifted and double-peak emission lines (Eracleous & Halpern 2003) will be observed at large angles of the BLR2 to the line of sight. Similar characteristics will have the narrow emission lines (Boroson 2005) ionized in the approaching subrelativistic outflow by the beamed continuum emission of the jet.

² On the assumption that the pattern speed and bulk speed of the jet of 3C 390.3 are equal, the jet inclination angle $\theta \sim 50^\circ$, bulk Lorentz factor $\gamma \sim 2$ and beaming angle $\psi \approx \gamma^{-1} \sim 30^\circ$ are estimated using the variable Doppler factor $\delta = 1.16$ (Lähteenmäki & Valtaoja 1999) and the maximum apparent speed of $1.5c$ observed in the compact jet.

The principal results of this work and its implications are:

1. Analysis of combined radio VLBI, optical/UV and X-ray data reveals significant correlations between variable optical continuum flux (5100Å) and radio flux density (15 GHz) of D and S1 stationary components of the jet (at the 99% and 95% confidence levels respectively). The optical emission follows the radio flares with the mean $\tau_{D-opt} \sim 1.4$ yr and $\tau_{S1-opt} \sim 0.4$ yr. This finding indicates for the physical link between the jet and optical continuum: the variable optical continuum emission is located in the innermost part of the jet near to component S1 and it is of non-thermal origin. This link is also supported by the correlation between the local maxima in the optical continuum light curve and the epochs at which the moving components of the jet pass the stationary radio feature S1.
2. These results have important implications for the structure of the sub-parsec-scale nuclear region. We suggest that (i) the characteristics of the long-term variability of optical continuum emission are related to the properties of the sub-parsec scale jet (ejection rate of the radio components, its structure and kinematics), (ii) the bulk of optical variable emission originates in the jet at a distance more than or equal to 0.4 pc from the central engine, and (iii) the continuum radiation of the jet forms two BLRs (associated with the jet and counterjet) in the subrelativistic outflow around the jet.

Acknowledgements. We acknowledge valuable discussions with N.G. Bochkarev. This work was supported by grants from CONACYT (Mexico), INTAS, FEBR and state program ‘Astronomy’ (Russia). The National Radio Astronomy Observatory is a facility of the National Science Foundation operated under cooperative agreement by Associated Universities, Inc.

References

- Alef, W., Wu, S. Y., Preuss, E., Kellermann, K. I., Qiu, Y. H. 1996, *A&A*, 308, 376
- Boroson, T. 2005, *AJ*, 130, 381
- Chiaberge, M., Capetti, A., & Celotti, A. 1999, *A&A*, 349, 77
- Chiaberge, M., Capetti, A., & Celotti, A. 2002, *A&A*, 394, 791
- Daly, R. A., Marscher, A. P. 1988, *ApJ*, 334, 539
- Dietrich, M. *et al.* 1998, *ApJS*, 115, 185
- Edelson, R. A., Krolik, J. H. 1998, *ApJ*, 333, 646
- Eracleous, M., & Halpern, J. P. 2003, *ApJ*, 599, 886
- Fabian, A. 1999, *Proc. Natl. Acad. Sci. USA*, 96, 4749
- Fabian, A. C. 2004, *astro-ph/0412224*
- Ferrari, A. 1998, *ARA&A*, 36, 539
- Field, G. B., Rogers, R. D. 1993, *ApJ*, 403, 94
- Gomez, J. L., Marti, J. M. A., Marscher, A. P., Ibanez, J. M. A., & Marcaide, J. M. 1995, *ApJ*, 449, L19
- Gomez, J. L., Marti, J. M. A., Marscher, A. P., Ibanez, J. M. A., Alberdi, A. 1997, *ApJ*, 482, L33
- Hardcastle, M. J., & Worrall, D. M. 2000, *MNRAS*, 314, 359
- Kaspi, S. *et al.* 2000, *ApJ*, 533, 631
- Kellermann, K. I. *et al.* 2004, *ApJ*, 609, 539
- Königl, A. 1981, *ApJ*, 243, 700
- Lähteenmäki, A., Valtaoja, E. 1999, *ApJ*, 521, 493
- Leighly, K. M. *et al.* 1997, *ApJ*, 483, 767
- Lobanov, A. P. 1998, *A&A*, 330, 79
- Marscher, A.P. *et al.* 2002, *Nature*, 417, 625
- Murray, N., Chiang, G. 1997, *ApJ*, 474, 91
- Mushotzky, R. F., Done, C., Pounds, K. A. 1993, *ARA&A*, 31, 717
- Pearson, T. J. 1997, in *ASP Conf. Ser.* 180, *Synthesis imaging in radio astronomy II*, eds. G. B. Taylor, C. R. Carilli, R. A. Perley, 335
- Peterson, B. M. 2002, *Advanced Lectures on The Starburst-AGN Connection*, eds Aretxaga, I., Kunth, D. & Mújica, R., Singapore World Scientific, 3
- Ponti, G., Cappi, M., Dadina, M., Malaguti, G. 2004, *A&A*, 417, 451
- Proga, D., Stone, J. M., Kallman, T. R. 2000, *ApJ*, 543, 686
- Romanova, M. M., Lovelace, R. V. E. 1996, *A&AS*, 120, 583
- Shapovalova, I. A. *et al.* 2001, *A&A*, 376, 775
- Sergeev, S.G., Pronik, V.I., Peterson, B.M., Sergeeva, E.A., Zheng, W. 2002, *ApJ*, 576, 660
- Ulrich, M., Maraschi, L., Urry, C. M. 1997, *ARA&A*, 35, 445
- Urry, C. M., Padovani, P. 1995, *PASP*, 107, 803
- Wamsteker, W., Ting-gui, W., Schartel, N., Vio, R. 1997, *MNRAS*, 288, 225
- Wandel, A., Peterson, B. M., Malkan, M. A. 1999, *ApJ*, 526, 579
- Worrall, D. M. 2005, *Multiband Approach to AGN*, eds Lobanov, A. P. & Venturi, T. *Memorie della Societa Astronomica Italiana*, 76, 28
- Zheng, W. 1996, *AJ*, 111, 1498

APPENDIX: Properties of the VLBA images and model fits of 3C 390.3

Table 1 compares the CLEAN component models (denoted ‘‘I’’) and Gaussian model fits (denoted ‘‘M’’) for the VLBA data used in the paper. The columns are: S_{total} – total flux density [mJy/beam]; S_{peak} – peak flux density [mJy/beam]; S_{min} – minimum flux density [mJy/beam]; χ^2 – goodness of the fit parameter; $\sigma_{rms,uv}$ – root-mean-square between the observed and model visibilities [mJy]. Last row presents average ratios between the respective image and model fit properties. The ratios are close to unity for the total and peak flux densities. The χ^2 parameter and the visibility r.m.s. are only slightly larger for the Gaussian model fits, which indicates that the model fits represent the structure adequately. The higher maximum negative flux density in the model fits (column S_{min}) indicates that the SNR of the Gaussian fits is on average 1.5 times lower than that of the VLBI images (due to increased non-Gaussian shapes of low-brightness regions). This reduction does not affect the fitted values of the component parameters (albeit it does increase the parameter errors) as it is related to extended emission associated with the underlying flow.

List of Objects

- ‘3C 390.3’ on page 2
‘3C 120’ on page 5

Table 1. Properties of the VLBA images and model fits of 3C 390.3.

Epoch	S_{total}		S_{peak}		S_{min}		χ^2		$\sigma_{\text{rms,uv}}$	
	I	M	I	M	I	M	I	M	I	M
1994.67	423.9	422.9	213.3	211.1	-2.2	-3.4	1.175	1.186	253.1	253.8
1995.96	463.1	466.2	190.8	190.8	-1.6	-2.8	0.328	0.334	119.2	120.3
1996.37	471.6	477.6	192.4	192.6	-1.3	-3.0	0.453	0.475	83.4	85.5
1996.82	389.5	399.1	174.2	174.2	-1.5	-3.2	1.235	1.504	42.5	45.2
1997.19	370.0	377.5	179.1	180.4	-0.7	-2.2	1.533	1.800	39.9	43.0
1997.66	418.3	425.2	267.4	267.2	-1.8	-2.2	0.575	0.580	152.1	152.5
1998.21	392.4	389.6	191.2	191.4	-1.1	-1.3	0.429	0.430	94.6	94.7
1999.85	313.2	315.8	216.9	218.6	-1.1	-1.3	1.103	1.149	31.0	31.4
2001.17	274.6	274.3	203.6	204.2	-1.1	-1.2	1.211	1.216	30.7	30.8
2002.13	308.8	303.6	208.4	210.3	-0.9	-1.2	1.020	1.146	26.5	27.8
< I/M >	0.994		0.998		0.664		0.943		0.977	